Finite Element Method for Hot cracking Using Interface Element†

Masakazu SHIBAHARA* , Hisashi SERIZAWA** and Hidekazu MURAKAWA***

Abstract

Based on the interface element proposed for crack propagation problems, a finite element method (FEM) using a temperature dependent interface element is developed. The proposed method is applied to the analysis of the occurrence and propagation of hot cracking in welding. In particular, the hot cracking extending from the starting end of the narrow rectangular plate under bead welding is examined using the proposed method. The following conclusions are drawn. In case of high welding speed with large heat input and small width of plate, hot cracking is likely to occur. This agrees with the phenomena generally observed in elements. The proposed method can simulate not only the occurrence and propagation of hot cracking, but also the contact of the starting edge of the plate after complete cooling.

KEY WORDS: (Hot cracking) (Solidification Brittleness) (Interface Element) (Temperature Dependency) (Surface Energy)

1. Introduction

In case of the FCB butt welding of a large-scale steel plate, hot cracking is frequently observed at the starting or finishing end of the plate[1]. X-ray or ultrasonic wave inspection is done to detect the cracking in these areas of the welding joint. Hot cracking with laser welding of aluminum alloy or stainless steel[2] has also been reported. In industry, hot cracking causes both increases of the production cost and the deterioration of products. Thus, it is important to reveal the mechanism of hot cracking formation in welding.

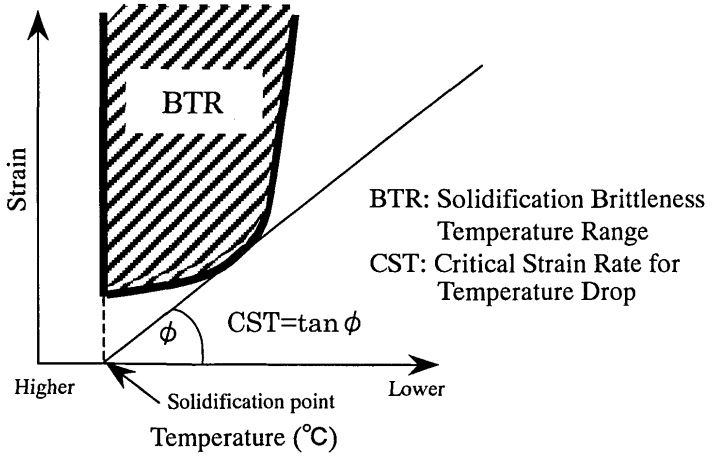

Fig.1 Schematic explanation of BTR and CST.

There have been many studies of hot cracking. For example, Senda *et al.*[3] proposed a parameter CST (critical strain rate for temperature drop) under the trans-varestraint test, which is considered as one of the most important parameters for sensitivity to hot cracking. The CST, which is dependent on both augmented strain and temperature, is defined as the slope of a tangent to BTR (solidification brittleness temperature range) from a solidification point, as shown in **Fig.1**. Most of the previous reports, however, involved experimental work and empirical formulae were proposed based on the experiments and they are not fully based on mechanical theory. Thus, in this study, the numerical code of a finite element method (FEM) is developed to clarify theoretically the mechanism of the hot cracking.

It is impossible to analyze hot cracking by a simple thermal elastic-plastic FEM code, such as has been used for analysis of the deformations and residual stresses under welding[4]. Conventional FEM models behavior of the volume by its nature. Hot cracking involves the formation of a new surface which must be modeled as a surface problem. Thus, it is essential to model the mechanical behavior of the surface in addition to that of the volume in order to analyze the formation and propagation of the hot crack. Recently, an interface element[5] was proposed based on the fact that the crack propagation can be

† Received on May 31, 1999
* Graduate Student, Osaka University
** Research Associate
*** Associate Professor

Transactions of JWRI is published by Joining and Welding Research Institute of Osaka University, Ibaraki, Osaka 567-0047, Japan.

considered as the formation of new surfaces, but the effects of temperature on the strength of the interface element were not taken into account. Therefore, in this research, a new temperature dependent interface element is developed and it is applied to analyze the hot cracking problem.

2. Theoretical Formulation

In case of ordinary crack propagation problems, a method using the interface element has been proposed. The mechanical behavior of the crack, in other words, the formation and the propagation of the crack, is governed by the interface potential ϕ per unit area of the crack surface. The requirements of the interface potential function are

(1) It involves the surface energy γ which is necessary to form the new surface as a material constant.
(2) It is a continuous function of opening displacement δ.

Among many functions satisfying these requirements, a Lennard-Jones type potential is employed. For application to hot cracking problem, the temperature dependency of the interface potential is introduced through the surface energy γ. Thus, the interface potential energy ϕ is defined by the following equation.

$$\phi(\delta, T) = 2\gamma(T)\left\{\left(\frac{r_0}{r_0+\delta}\right)^{2n} - 2\left(\frac{r_0}{r_0+\delta}\right)^{n}\right\} \quad (1)$$

Where $\gamma(T)$ is the surface energy per unit area which is temperature dependent. n and r_0 are the constants independent of the temperature.

The derivative of ϕ with respect to the crack opening δ as shown in the following equation gives the bonding strength per unit area of the crack surface.

$$\sigma = \frac{\partial\phi}{\partial\delta} = \frac{4\gamma n}{r_0}\left\{\left(\frac{r_0}{r_0+\delta}\right)^{n+1} - \left(\frac{r_0}{r_0+\delta}\right)^{2n+1}\right\} \quad (2)$$

Further, the bonding strength per unit area becomes a maximum under the following condition.

$$\frac{\delta}{r_0} = \left(\frac{2n+1}{n+1}\right)^{\frac{1}{n}} - 1 \quad (3)$$

The maximum bonding strength σ_{cr} is given by,

$$\sigma_{cr}(T) = \frac{4\gamma n}{r_0}\left\{\left(\frac{n+1}{2n+1}\right)^{\frac{n+1}{n}} - \left(\frac{n+1}{2n+1}\right)^{\frac{2n+1}{n}}\right\} \quad (4)$$

Where σ_{cr} gives the critical strength at temperature T. Since σ_{cr} is proportional to $\gamma(T)$ as shown by **Eq.(4)**, the temperature dependency of the surface energy γ is directly reflected in the critical strength σ_{cr}.

2.2 Load Vector and Stiffness Matrix in Temperature Dependent Interface Element

In this chapter, load vector and stiffness matrix are introduced. Before this chapter, balanced equations should be introduced, but this is written in a reference[3], so this is omitted.

Temperature dependent interfacial potential energy is given in **Eq.(5)**.

$$U_s^e(u_0^e, T) = \int\phi(\delta, T)dS^e \quad (5)$$

Where, u_0 shows nodal displacement, T shows temperature and δ shows opening displacement. In **Eq.(6)**, $U_s^e(u_0^e + \Delta u_0^e, T + \Delta T)$ is transformed with Talor's expansion about Δu_0^e and ΔT.

$$U_s^e(u_0^e + \Delta u_0^e, T + \Delta T) = \int\phi(\delta + \Delta\delta, T + \Delta T)dS^e$$

$$= \int\phi dS^e + \int[\frac{\partial\phi}{\partial\delta}\{\frac{\partial\delta}{\partial u_0^e}\}^T + \frac{\partial^2\phi}{\partial\delta\partial T}\{\frac{\partial\delta}{\partial u_0^e}\}^T\Delta T]\{\Delta u_0^e\}dS^e$$

$$+\frac{1}{2}\int(\frac{\partial^2\phi}{\partial\delta^2} + \frac{\partial^3\phi}{\partial^2\delta\partial T}\Delta T)\{\Delta u_0^e\}^T\{\frac{\partial\delta}{\partial u_0^e}\}\{\frac{\partial\delta}{\partial u_0^e}\}^T\{\Delta u_0^e\}dS^e + H.O.T. \quad (6)$$

First order term and second order term about increment of nodal displacement Δu_0^e are arranged to these equations.

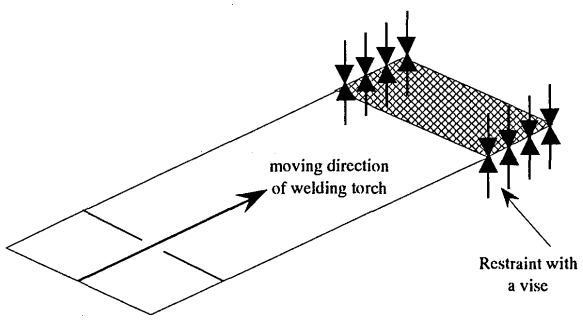

Fig.2 Schematic illustration of experiment.

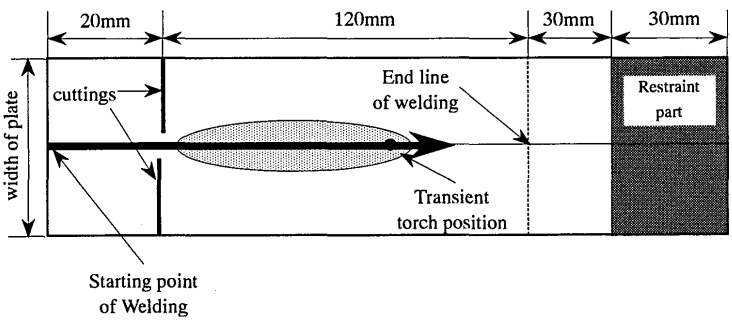

Fig.3 Shape and size of test specimen.

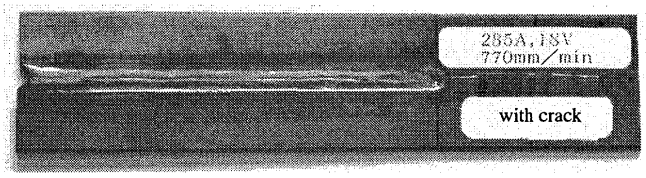

(a) overall picture

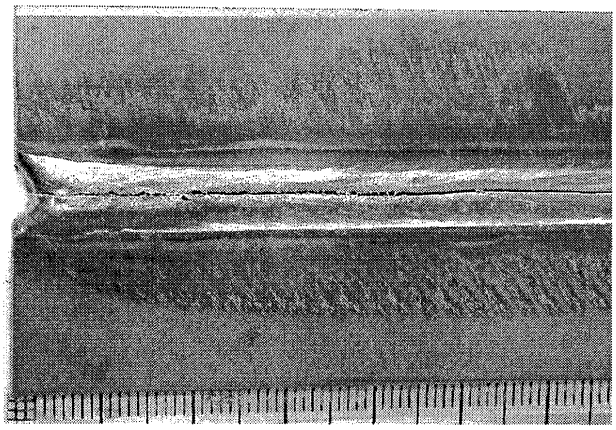

(b) enlarged view

Fig.4 Test specimen after welding (with crack).

$$\int\left(\frac{\partial\phi}{\partial\delta}\left\{\frac{\partial\delta}{\partial u_0}\right\}^T+\frac{\partial^2\phi}{\partial\delta\partial T}\left\{\frac{\partial\delta}{\partial u_0}\right\}^T\Delta T\right)\{\Delta u_0^e\}dS^e=-\{f\}^T\{\Delta u_0^e\} \quad (7)$$

$$\frac{1}{2}\int\left(\frac{\partial^2\phi}{\partial\delta^2}+\frac{\partial^3\phi}{\partial^2\delta\partial T}\Delta T\right)\left(\frac{\partial\delta}{\partial u_0}\right)^2(\Delta u_0{}^e)^2dS^e$$

$$=1/2\{\Delta u_0\}^T[K]\{\Delta u_0\} \quad (8)$$

Load vector {f} and stiffness matrix [K] in temperature dependent interface element are as coefficients of first order term and second order term. That is,

$$\{f\}=-\int\left(\frac{\partial\phi}{\partial\delta}\left\{\frac{\partial\delta}{\partial u_0}\right\}^T+\frac{\partial^2\phi}{\partial\delta\partial T}\left\{\frac{\partial\delta}{\partial u_0}\right\}^T\Delta T\right)dS^e \quad (9)$$

$$[K]=\int\left(\frac{\partial^2\phi}{\partial\delta^2}+\frac{\partial^3\phi}{\partial^2\delta\partial T}\Delta T\right)\left\{\frac{\partial\delta}{\partial u_0}\right\}^T\left\{\frac{\partial\delta}{\partial u_0}\right\}dS^e \quad (10)$$

3. Experiment of Starting End Cracking Under Bead Welding

The end cracking observed at both the starting end and the finishing end of the FCB butt weld joint between large plates are typical examples of hot cracking. Although, hot cracking sensitivity of mild steel is low, hot cracking can be produced in a small-scale laboratory test specimen when the welding

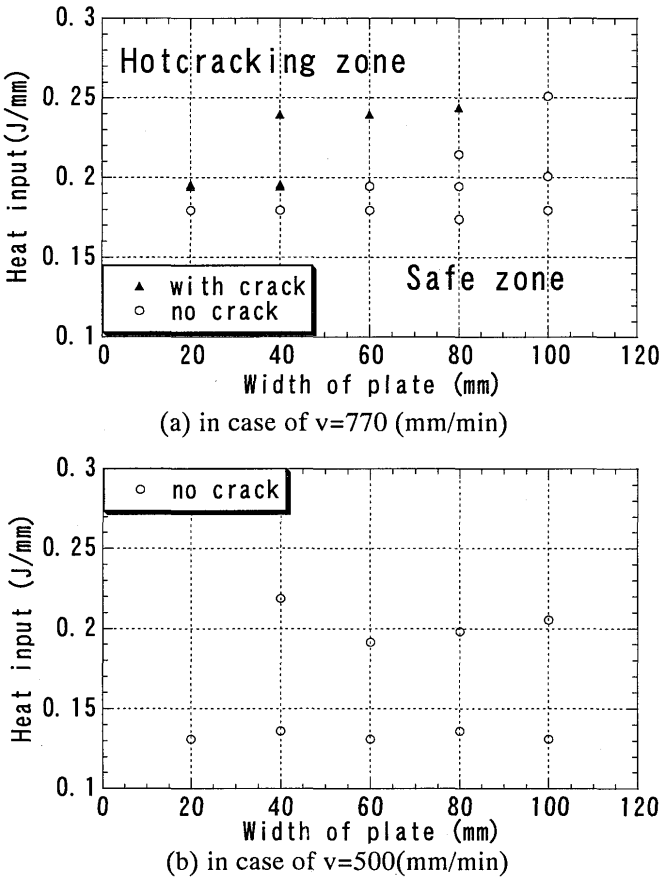

Fig.5 Effect of heat input and width of plate on hot cracking (experiment).

conditions and geometry of the specimen are properly chosen. As in the case of FCB welding, two forms of end cracking, namely cracking at the starting end and the finishing end, are possible in the laboratory test. In the present report, end cracking at the starting end is studied. A series of experiments using bead welding on rectangular plate are conducted for the following purposes,

(1) to clarify the effect of the width of the plate, which represents the degree of restraint, on the hot cracking,
(2) to clarify the effect of welding conditions on the occurrence of hot cracking,
(3) to provide reference data for the verification of the proposed method of analysis.

Figure 2 is a schematic illustration of the experiment on hot cracking with bead welding. The specimen is fixed at one end by a vice so it is lifted in the air. The plate is melted by the TIG torch starting from the free end toward the fixed end. A tab plate is built in the specimen with a pair of slits. The tab plate is designed to be melted off when the torch reaches the position of the slit so that uniform heat input throughout

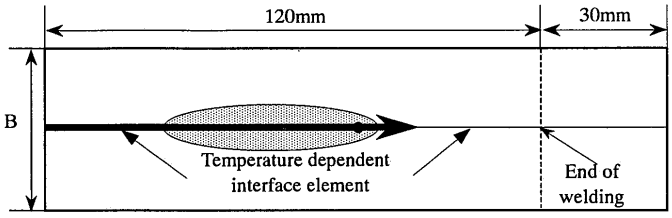

Fig.6 Model for analysis.

Fig.7 FEM mesh division (half model).

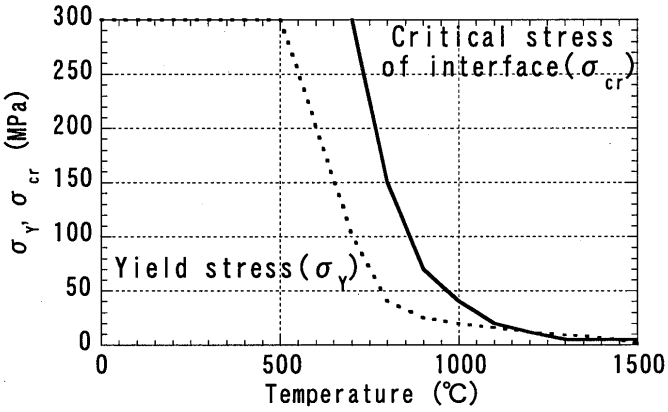

Fig.8 Temperature dependence of yield stress(σ_y) and critical stress of interface.

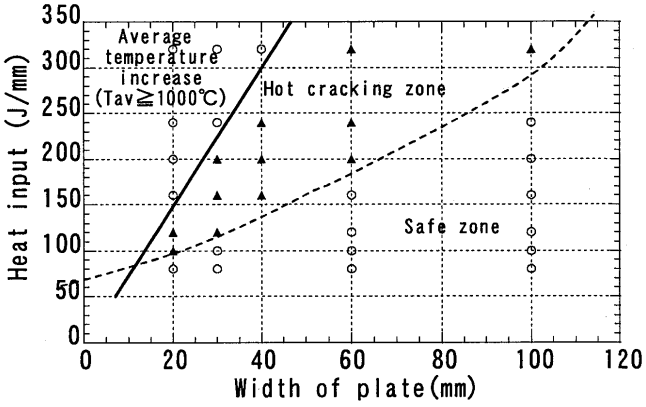

(a) in case of v=1500(mm/min)

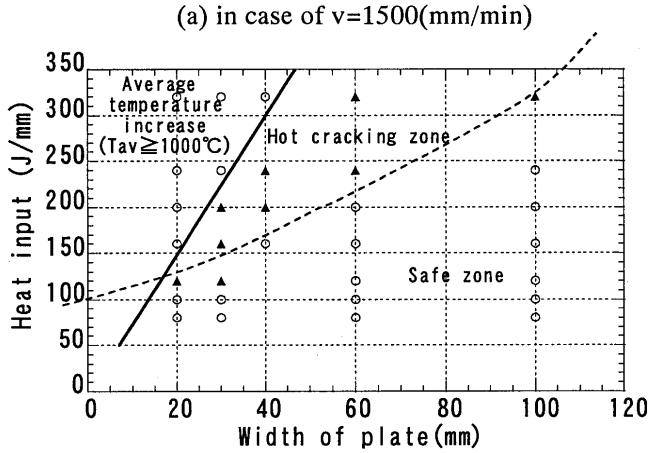

(b) in case of v=1000(mm/min)

Fig.9 Effect of heat input and width of plate on ho cracking (computation).

the welding line, including the starting point, can be achieved. The exact dimensions of the specimen are shown in **Fig. 3**. In the experiment, the width of the specimen, the welding speed and the heat input are changed to examine the effect of these parameters. The net heat input Q is estimated from the welding current I, the welding voltage V and the welding speed v using the following equation.

$$Q=\eta(VI/v) \qquad (11)$$

where, η is the heat input efficiency and it is assumed to be 0.6 for TIG welding. **Figure 4** shows an example of specimens in which the cracking is observed. The width of the specimen is 40 mm and the welding speed, the current and the voltage are 770 mm/min, 255 A and 18 V, respectively. The experiments are conducted with two welding speeds, namely 770 mm/min and 500 mm/min. The result of the experiments is summarized in **Fig. 5**. The specimens with crack and without crack are s distinguished by solid triangles and open circles. As seen from the figure, no crack is observed when the welding speed is low. When the welding speed is high, cracking is observed in specimens with high heat input and small width.

From the result of the experiments, it is generally concluded that cracking is likely to occur when the width of the specimen is small, the welding speed is high and the heat input is large. The width of the specimen corresponds to the constraint on the deformation of the opening mode at the weld due to the thermal deformation of the plate. On the other hand, a high welding speed and heat input produce longer melting zones behind the welding torch. When the length of the melting zone is large, the resistance to the opening deformation of the weld becomes small. Thus, the combination of the small width of the specimen and the long melting zone promotes the occurrence of cracking.

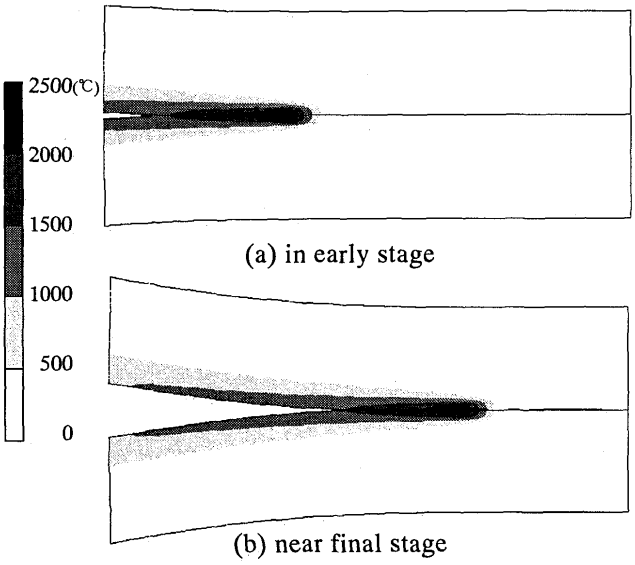

Fig.10 Transient temperature distribution and deformation (B=60mm,v=1500mm/min,Q=200J/mm).

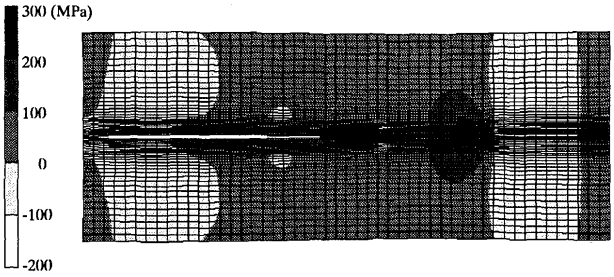

Fig.11 Stress(σ_y) distribution and deformation after Complete cooling (B=60mm,v=1500mm/min,Q=200J/mm).

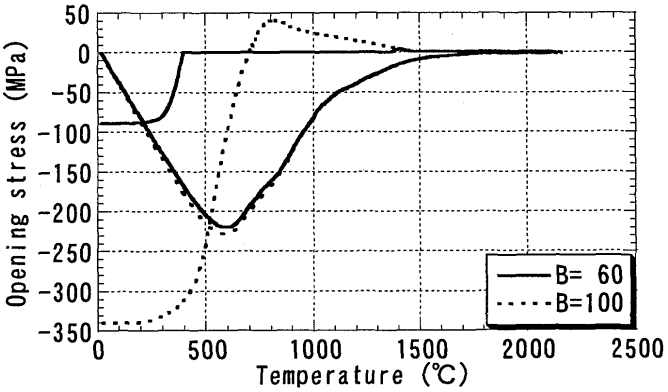

Fig.12 Opening stress(σ_y) in thermal cycle on interface element at the starting edge of welding line (v=1500mm/min,Q=200J/mm).

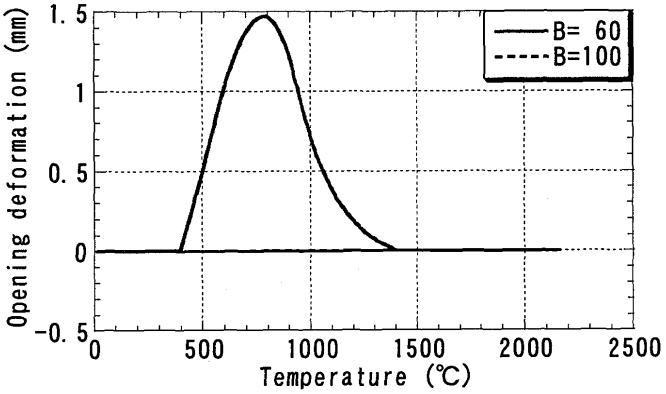

Fig.13 Opening deformation in thermal cycle on interface element at the starting edge of welding line (v=1500mm/min,Q=200J/mm).

4. Simulation

4.1 Model for analysis

To clarify the validity of the proposed method for the analysis of hot cracking during welding, the same model used for the experiment is analyzed. Further, the mechanical phenomena are closely examined based on the computed results. The model and the mesh division employed in the analysis are shown in **Figs. 6** and **7**, respectively. Because of the symmetry of the problem, only the half of the specimen is analyzed. The interface elements representing the potential crack are arranged along the center of the welding line. **Figure 8** shows the temperature dependency of σ_{cr} which is an important parameter controlling the occurrence of hot cracking. As shown in Fig. 8, the critical stress σ_{cr} becomes smaller than the yield stress between 1200 ℃ and 1450 ℃. This temperature range corresponds to the solidification brittleness temperature rang (BTR). The parameter r_0 and n in the interface potential energy function defined by **Eq.(1)** are assumed to be 0.025 and 6.0, respectively.

4.2 Computed results

The computed results are summarized as in the same manner as those for the experiments. **Figures 9(a)** and **(b)** show the effects of the heat input and the width of the specimen on the occurrence of hot cracking for cases in which the welding speeds are 1500 mm/min and 1000 mm/min, respectively. When a large heat input is applied to a narrow plate, the average temperature of the specimen becomes higher than 1000 ℃. Thus, such cases indicated in Figs. 9(a) and (b) can be excluded as unrealistic cases. Ignoring these cases, from Fig.9, it can be seen that hot cracking is likely to occur in the case of larger heat input and smaller width of the specimen. It is also seen from the comparison between Figs. 9(a) and (b) that the hot cracking is promoted when the welding speed is fast.

The transient temperature distributions and

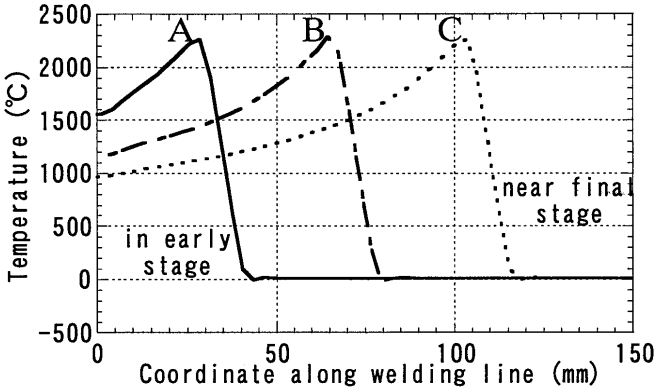

Fig.14 Temperature distribution along welding line (B=60mm,v=1500mm/min,Q=200J/mm).

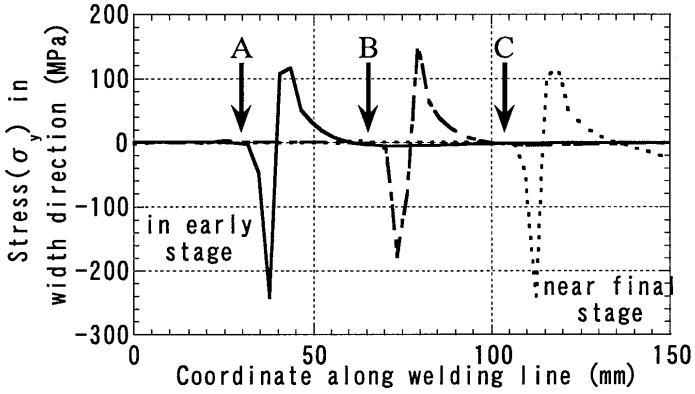

Fig.15 Distribution of stress(σ_y) in breadth direction along welding line (B=60mm,v=1500mm/min,Q=200J/mm).

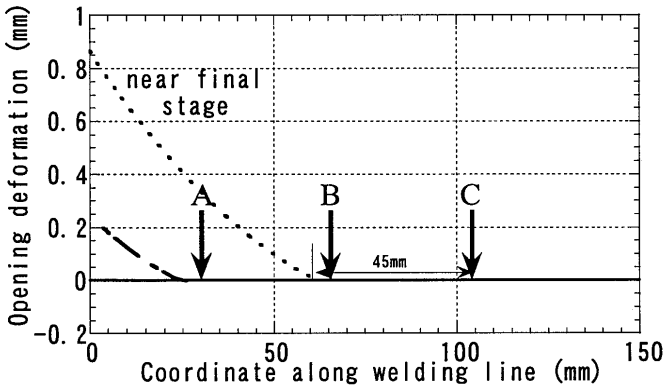

Fig.16 Opening deformation along welding line (B=60mm,v=1500mm/min,Q=200J/mm).

deformations in the early stage and near the final stage are shown in **Figs.10(a)** and **(b)**. Once the crack is initiated, the opening deformation of the crack becomes larger as the movement of the welding torch. **Figure 11** shows the deformation and the distribution of the stress component normal to the welding direction after complete cooling. The crack is closed during cooling and the starting end is closed after the complete cooling.

Since the cracking studied in the present work is typical mode-I cracking, the stress and the deformation in the opening mode are closely examined to clarify the mechanism. The histories of the opening stress (stress component normal to the welding direction) and the opening displacement at the starting end during the thermal cycle are shown in **Figs. 12** and **13**. In these figures, the wide specimen without cracking and the narrow specimen with cracking are compared. The widths of the specimen are 100 mm and 60 mm and they are welded with the same conditions. As seen from Fig.12, the stress in the cooling stage becomes tensile at about 700 ℃, which is well below the BTR when B=100 mm. Hot cracking does not occur in this case. When B=60 mm, the stress becomes tensile at about 1450 ℃ which is in the BTR. The crack is formed at this moment as seen from **Fig.13**. The starting end is closed at about 450 ℃ and the compressive stress appears due to the contact. These results demonstrates the ability of the proposed method to simulate the surface phenomena precisely, including the contact between the cracked surfaces and in addition to the formation and the extension of the hot crack.

Figure 14 shows the temperature distributions along the welding line in the early stage, the intermediate stage and the final stage, respectively. The points A, B and C indicate the points with the maximum temperature in each stage. The distributions of the stress component normal to the welding direction along the welding line in the three stages are shown in **Fig.15**. At the position of the heat source, the compressive stress appears because of thermal expansion. The region with tensile stress extends ahead of the heat source to maintain the balance of stress. Behind the heat source, the tensile stress zone appears just after the region with small compressive stress. The tensile stress in this zone is generally small. But, the crack is formed if the opening stress exceeds the critical stress σ_{cr} of the interface element. Such points where the crack is formed are located about 45 mm behind the heat source as shown in **Fig. 16**.

5. Conclusions

In order to clarify the mechanism of the hot cracking theoretically, a FEM analysis with a temperature dependent interface element is developed

and it is applied to the analysis of hot cracking. The conclusions can be summarized as follows;

(1) The proposed method can be applied to the analysis of hot cracking at the starting end of the rectangular plate under the bead welding.

(2) The computed results show that hot cracking is likely to occur when the heat input is high, the welding speed is large and the width of the plate is small. This tendency predicted by the analysis agrees well with experiment.

(3) The proposed method can simulate not only the occurrence and the propagation of hot cracking, but also the contact at the starting end of the plate after complete cooling.

References

1) K.Satoh, Y.Ueda, T.Maeda, T.Yada, R.Kamichika, Y.Kim: Studies on Deformation and Cracking in One Sided Welding (Ist Report), Bulletin of Society of Naval Architects of Japan , No.136(1974-11)

2) K.Shinozaki: Weld Cracking of Ni-base Superalloys During Laser Welding, Preprints of the meeting of J.W.S, No.62(1998-4)

3) T.Senda, F.Matsuda: Studies on Solidification Crack Susceptibility for Weld Metals with Trans-Varestraint Test (1), Trans of J.W.S, No.41-6(1972)

4) M.Shibahara, H.Murakawa: Effect of Various Factors on Transverse Shrinkage under butt welding, Journal of the KSNAJ, No.230(1998-9)

5) Z,Wu, H.Murakawa: Computer Simulation Method for Crack Growth Using Surface Energy and Its Application to Interface Stripping of Composite Material(1st Report), Journal of the KSNAJ, No.230(1998-9)